ARTICLES

# Bichromophoric Interactions and Time-Dependent Excited State Mixing in Pyrene Derivatives. A Femtosecond Broad-Band Pump−Probe Study

**M. Raytchev,[†] E. Pandurski,[†] I. Buchvarov,[‡] C. Modrakowski,[§] and T. Fiebig*,[†]**

*Institut für Physikalische und Theoretische Chemie, Technische Universität München, Lichtenbergstrasse 4, D-85748 Garching, Germany, Department of Quantum Electronics, Sofia University, J. Bouchier Blvd. 5A, 1164 Sofia, Bulgaria, and Institut für Chemie, Freie Universität Berlin, Takustrasse 3, D-14195 Berlin, Germany*

*Received: October 31, 2002; In Final Form: February 26, 2003*

Femtosecond broad-band pump−probe spectroscopy has been used to study intramolecular bichromophoric coupling and structural relaxation in pyrene and aryl pyrene derivatives in solution. The influence of aryl substituents on the $S_2 \rightarrow S_1$ internal conversion process, which occurs with a time constant of ∼75 fs in pyrene, has been investigated. While in 1-phenylpyrene the internal conversion is faster than 50 fs, it is slower in 1-biphenyl-4-yl-pyrene (105 fs). The temporal evolution of the transient absorption spectrum indicates strong mixing of several “zero-order” electronic configurations—which evolve separately with time—in the $S_1$ and the $S_2$ states. The time-resolved spectra are interpreted within the framework of an adiabatic state model which includes interchromophoric electronic coupling. In this paper we give a full description of the experimental setup, the data acquisition procedure, and several experimental details about the characterization of the broad-band femtosecond white light source.

## I. Introduction

Understanding electronic communication between chromophores in complex molecular architectures is key for the design and construction of functional nanoscale photonic devices.[1,2] Such communication is based on interchromophore electronic coupling which mediates electron and/or excitation energy transfer.[3−7] In addition to interchromophore transfer processes, there are intrachromophore radiationless transitions which compete with energy and electron transfer. To investigate the interplay between electronic and vibronic relaxation mechanisms, advanced spectroscopic techniques can be applied to monitor the ultrafast molecular dynamics on the time scale of the nuclear motion.[8,9]

Since the discovery of excimer formation by Förster and Kasper in 1954,[10] pyrene has been used as a chromophore in various charge and energy transfer systems, both to investigate the nature of elementary photophysical processes[11−20] and to probe structure and dynamics in biological systems.[21−26] Despite the vast number of pyrenyl donor (D)−acceptor (A) systems reported, the excited state dynamics of pyrene are still not completely understood. It is generally assumed that the initially excited state—often referred to as the locally excited state (LE) in D/A assemblies—is the $S_1$ state ($^1B_{2u}$; short axis polarized) of pyrene. Although the $S_0 \rightarrow S_1$ transition has a vanishing extinction coefficient[27] and excitation into the long-wavelength absorption band in solution generally populates the $S_2$ state ($^1B_{1u}$; long axis polarized), it is widely assumed that the $S_2 \rightarrow S_1$ internal conversion (IC) is faster than subsequent photochemical processes. The origin of the ultrafast IC lays in the small energy gap (∼2700 $\mathrm{cm}^{-1}$ in hydrocarbon solution[28]), which allows efficient vibronic coupling.[28−31] This assumption is certainly valid for intermolecular D/A systems where the charge transfer (CT) is limited by diffusional motion.[11,12,14] However, when a $\pi$-conjugated donor or acceptor moiety is directly linked to pyrene (e.g. through a single $\sigma$-bond), the two low-lying excited states are perturbed and the electronic nature of the LE state becomes unclear.[32]

In this paper we present our broad-band femtosecond pump−probe method which has been designed to monitor the spectral evolution after optical pumping in (multi)chromophoric systems. Focusing on the bichromophoric interactions in pyrene derivatives, we demonstrate how excited-state spectra can provide information about the composition of excited-state wave functions and, therefore, about time and conformationally dependent electronic coupling in multichromophores. Moreover, we will focus on the $S_2 \rightarrow S_1$ IC process in pyrene, which is an intrinsic part of the excited-state dynamics in all pyrenyl molecular architectures. We investigated the IC dynamics in three pyrene derivatives (see Chart 1) and studied the influence of the aryl substituents on the nature of this process.

The paper is structured in the following way. In section II we give a detailed description of our experimental setup and explain the data acquisition and analysis procedures. In section III we present steady state and femtosecond time-resolved data of pyrene (**P**), 1-phenylpyrene (**Ph-P**), and 1-biphenyl-4-yl-

---

* Corresponding author. E-mail: Fiebig@ch.tum.de. Fax: +49 89 289 13244.

[†] Technische Universität München.

[‡] Sofia University.

[§] Freie Universität Berlin.

10.1021/jp027356c CCC: $25.00

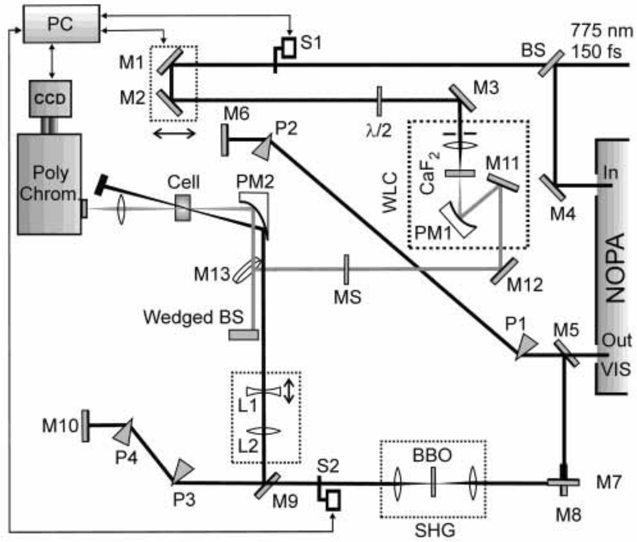

**Figure 1.** Schematic representation of the experimental setup. The following notations have been used: BS, beam splitter of the fundamental 775 nm beam; shutter 1 and shutter 2, two motorized shutters which block the probe and pump beams, respectively; M1, M2, M3, and M4, high reflection dielectric mirrors at 775 nm, 45°; $\lambda/2$, a $\lambda/2$ plate; $CaF_2$, calcium fluoride plate, used for white light continuum (WLC) generation; M5, M6, M7, M8, M9, M10, M11, M12, and M13, aluminum mirrors; PM1, 30° off-axis parabolic mirror; PM2, 90° off-axis parabolic mirror; MS, dielectric mirror used to cut off the fundamental; wedged BS, wedged beam splitter, used to split the WLC into probe and reference beams; P1, P2, P3, and P4, fused silica prisms; L1 and L2, lenses with focal lengths −50 and 75 mm, respectively.

**CHART 1**

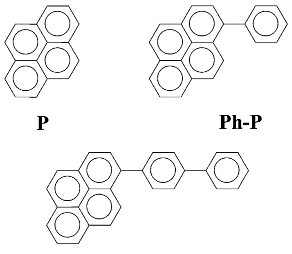

**P** **Ph-P**

**BPh-P**

pyrene (**BPh-P**) and address a fundamental experimental problem regarding femtosecond measurements in solution. In section IV we will present a model to describe the spectral and dynamical features observed in **Ph-P** and **BPh-P** based on the spectroscopic properties of pyrene and intramolecular bichromophoric coupling. Within the frame of this model we derive structural information directly from the time-dependent evolution of the transient spectra. Finally, we discuss the implications of this study on the description of ultrafast charge-transfer processes in conjugated molecular assemblies.

## II. Experimental Section

**A. Femtosecond Experimental Setup and Data Acquisition.** A detailed schematic of our femtosecond pump−probe spectrometer is shown in Figure 1. A fraction of the output of a commercial titanium/sapphire amplifier system (Clark-MXR, Inc., CPA-2001, 775-nm, 150 fs, 800 $\mu$J, 1 kHz) is split into two beams with energies of 4 and 230 $\mu$J, respectively. The high energy beam is used to pump a commercial two stage visible noncollinear optical parametric amplifier (NOPA). The output of the NOPA is a chirped broad-band pulse, tunable between 450 and 700 nm with energies of about 5−15 $\mu$J which is compressed using a two prism (P1 and P2) compressor.[33] The resulting pulse durations—measured by a commercial autocorrelator—are typically between 20 and 40 fs fwhm (assuming Gaussian pulse shape). Tunable femtosecond pulses in the UV region are available through second harmonic generation of the NOPA output in a 100 $\mu$m thick BBO crystal (type I phase matching) and subsequent compression.[34] To minimize Fresnel losses in the compressor prisms (P3 and P4), the polarization of the second harmonic must be horizontal. Hence, the NOPA output polarization before the doubling crystal is changed from horizontal to vertical by a pair of mirrors M7 and M8.

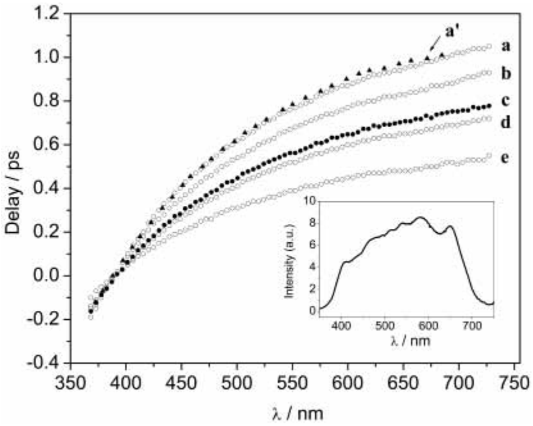

**Figure 2.** Chirp measurements of the white light continuum (WLC) using the cross phase modulation (XPM) artifact (a-d) and the up-conversion technique (a′) in a 100 $\mu$m thick nonlinear BBO crystal: a and a′, after propagating through a 1 mm cell, filled with solvent; b, after propagating through an empty cell (2 mm × 1.25 mm); c, resulting chirp used for the time correction (c = d + (a − b)/2); d, after propagating through a single cell wall (1.25 mm fused silica); e, in the absence of a cell. The inset shows the spectrum of the WLC (linear intensity scale).

The optical density changes induced by optical pumping in the sample are probed by a delayed femtosecond white light continuum (WLC) generated by tightly focusing the lower energy beam (4 $\mu$J) into a 3 mm thick rotating $CaF_2$ plate. Collimation of the wide spectrum is performed by a 30° off-axis parabolic mirror PM1 with an off-axis focal length of 77 mm. Depending on the alignment, the WLC provides a usable probe source between 320 and 750 nm. A dielectric mirror MS with a customized multilayer coating is used for attenuation of the fundamental (775 nm) and to smooth the probe spectrum (see inset of Figure 2).

After it passes the mirror MS, the WLC is split into two beams—probe and reference—using a wedged beam splitter. The reference beam is directed through a sample volume which is not affected by the pump pulse. Both the probe and reference spectra are detected independently and simultaneously by a CCD array. Pump, probe, and reference beams are focused in the sample by a 90° off-axis parabolic mirror with an off-axis focal length of 100 mm. The angle between pump and probe beam is kept below 5°. The pump beam spot size into the sample is controlled by varying the distance between two lenses (L1 and L2) with focal lengths 75 and −50 mm. Typical pump spot sizes are 200−600 $\mu$m. The pump energy varies between 200 and 800 nJ, depending on the pump wavelength. The detection system consists of an imaging polychromator (TRIAX 180, Jobin Yvon) and a CCD array (Hamamatsu, S7031) cooled to −20 °C using a multistage TEC system.

To improve the sensitivity of the measurement, a dual beam geometry (probe and reference) and a four-step measurement cycle have been implemented. At each step the probe and reference signals are recorded under conditions determined by the state of the shutters S1 and S2 (S1, shutter (open/close) for the probe and reference beams; S2, shutter (open/close) for the pump beam).

The recorded signals at each step result from averaging of, typically, several hundred laser pulses. The exact number of acquired laser shots within a single four-step cycle is changeable and depends on individual experimental conditions.

The overall sensitivity, that is, the smallest signal change that can be measured, is typically 0.2 mOD (1 mOD = $10^{-3}$ optical density units). The signal at negative delay (so-called baseline) is in the range ±2 mOD. Since it is independent of the delay, it is subtracted from the data.

**B. Characterization of the WLC Chirp.** The WLC pulse passes through the $CaF_2$ plate and subsequent optical elements, which introduce a chirp due to the group velocity dispersion (GVD); that is, the different spectral components of the WLC accumulate different group delays. As a result, different spectral components of the WLC pulse are interacting with the excited sample molecules at different delay times. Before entering the sample, the WLC is spread in time, typically from several hundred femtoseconds up to picoseconds, depending on the length of dispersive material it has passed through. Hence, to correct the wavelength dependence of "time-zero" in pump−probe experiments, one has to characterize the group delays of the different spectral components of the WLC very accurately.

All chirp-measurement techniques are based on $\chi^{(2)}$ and $\chi^{(3)}$ type nonlinear interaction between the WLC and a gate pulse.[35−39] Recently, there have been reports about a method using a cross-phase modulation (XPM) artifact signal which is generated by the interaction of pump and probe pulses in the sample medium.[36,38−40] This XPM artifact provides a very convenient way to characterize the chirp because the measurement can be carried out in the same experimental arrangement as used for measuring the pump−probe spectra. However, the physical phenomenon which results from XPM is very complicated. An approximate description of the XPM artifact can be given assuming Gaussian shaped wave packets and a linear chirp of the phase modulation function. In this case, the artifact behavior depends strongly on the product of chirp rate and the square of the pump pulse duration.[38,39] Unfortunately, this simplified description does not guarantee a universally valid prediction of XPM artifacts under real experimental conditions. In addition, we observed a substantial decrease in the accuracy of the group delay measurements going from the blue to the red part of the WLC.[41] Therefore, we used a second method based on sum-frequency generation between a gate pulse and the WLC[37] to verify the results of the XPM artifact measurements. For the sum-frequency generation we used a 100 $\mu$m thick BBO crystal (32° cut) and a gate pulse (35 fs, 675 nm, 5 $\mu$J) from the NOPA. The sum-frequency was detected using a commercial spectrograph (Ocean Optics USB2000). To obtain the XPM artifact signal, we used the frequency-doubled NOPA output as a gate pulse (345 nm) and focused it into the BBO crystal. Figure 2 (a and a′) shows that both methods give similar results (within 7%). The temporal accuracy of the chirp measurement is better than 15 fs. The accumulated group delay of the different spectral components of the WLC probe in the sample is obtained by measuring the chirp of the WLC in the presence and absence of the cell and the solvent (see Figure 2b−e).

**C. Data Analysis.** From the chirp characterization we obtain the relative time delay values between probe wavelengths. Hence, the temporal evolution of the entire pump−probe spectrum can be constructed by applying the proper time-shift correction.[42] However, for a quantitative analysis of the data we need to determine the absolute time-zero values with respect to the pump pulse. This is realized by numerical deconvolution of an instantly rising spectral component $F_\lambda(t)$ at a certain wavelength with the response function of our experimental setup, which is assumed to be Gaussian: $g(t) = 1/(\pi^{1/2}\sigma)\exp[-\{(t - \tau_0)/\sigma\}^2]$. $F_\lambda(t)$ is a sum of up to four exponentials:

$$F_\lambda(t-\tau) = \sum_i c_i e^{-(t-\tau)/\tau_i} \quad (t-\tau \geq 0) \tag{1}$$

The resulting time-dependent signal (at a given probe wavelength $\lambda$) $S_\lambda(t)$ is given by

$$S_\lambda(t) = \int_{-\infty}^{t} g(\tau) F_\lambda(t-\tau)\, d\tau \tag{2}$$

which can be solved analytically to give

$$S_\lambda(t) = \sum_i c_i \frac{1}{2} \exp\left[-\frac{1}{\tau_i}\left(t - \tau_0 - \frac{\sigma^2}{4\tau_i}\right)\right] \times \left\{1 - \mathrm{erf}\left[\left(t - \tau_0 - \frac{\sigma^2}{2\tau_i}\right)\frac{1}{\sigma}\right]\right\} \tag{3}$$

where erf is the error function and $c_i$ is the amplitude of the component ($i$) with decay time $\tau_i$. The full width at half-maximum (fwhm) of the experimental response ($\tau_M$) is related to $\sigma = \tau_M/1.6651$. Here $\tau_0$ is the time shift, which is subsequently used to determine the absolute time-zero. The parameters $\tau_i$, $\tau_M$, and $\tau_0$ can be evaluated using the least-squares fitting procedure of eq 3.

**D. Samples.** The solvents were Uvasol grade (Merck) and were used without further purification. Pyrene (**P**) was purchased from Fluka (fluorescence grade) and used without further purification. 1-Phenylpyrene (**Ph-P**) was synthesized, characterized, and purified by Dr. Wolfgang Kühnle at the Max Planck Institute for Biophysical Chemistry. The synthesis of **Ph-P** has been recently described in ref 17. The synthesis of 1-biphenyl-4-ylpyrene (**BPh-P**) was carried out using the Suzuki coupling reaction and is fully described in the Supporting Material.

The time-resolved experiments were carried out using two types of sample cells with optical path lengths of 1 mm and 100 $\mu$m. Both cell types had 1.25 mm thick fused silica windows. For the steady-state measurements we used a 10 mm thick cell. Steady-state fluorescence spectra were obtained with a Fluoromax-3 fluorimeter. The spectra were intensity corrected. The absorption spectra were recorded with a Varian Cary 50 spectrometer. The sample concentrations were between $\sim 10^{-4}$ M (1 mm cell) and $\geq 10^{-3}$ M (100 $\mu$M cell).

To exclude the formation of pyrenyl radical cations due to multiphoton excitation, we recorded spectra with different pump intensities and obtained no significant changes in the relative intensities of the transient absorption bands. In accord with this fact, we did not observe degradation of the sample during the measurement. Finally, steady-state absorption and fluorescence spectra of the samples measured before and after the time-resolved experiments were compared with each other and no indications of degradation were found.

## III. Results

### A. Steady-State Absorption and Fluorescence Spectra.

Figure 3 shows the steady-state absorption and emission spectra

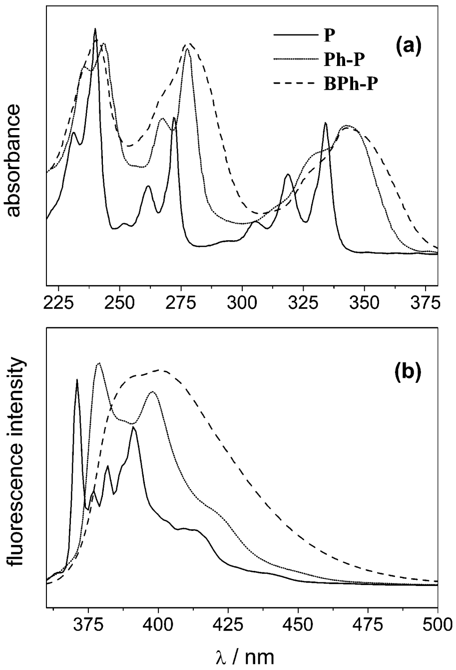

**Figure 3.** Steady-state absorption (upper panel) and fluorescence spectra (lower panel) of **P**, **Ph-P**, and **BPh-P** in acetonitrile.

of **P**, **Ph-P**, and **BPh-P** dissolved in acetonitrile. The absorption spectra exhibit the characteristic vibronic structure of pyrene in solution. However, for **Ph-P** and **BPh-P** we observe substantial spectral broadening and bathochromic shifting of the absorption bands. In particular, the $S_0 \rightarrow S_2$ transition of pyrene (**P**) with its 0−0 transition at 334 nm is red-shifted in **Ph-P** and **BPh-P** by almost 10 nm (780 $\mathrm{cm}^{-1}$). Moreover, the line shape of this vibronic transition in **P** has a sharp Lorentzian profile with a fwhm of ∼450 $\mathrm{cm}^{-1}$. In **Ph-P** and **BPh-P** the line shape deviates from the Lorentzian profile and the width is strongly increased. While unsubstituted pyrene (**P**) shows a pronounced vibrational structure in its fluorescence, the spectra of **Ph-P**, and particularly of **BPh-P,** are less structured. These observed changes in the absorption spectra give strong evidence for inhomogeneous spectral broadening in **Ph-P** and particularly in **BPh-P**, which is likely to be induced by the conformational flexibility of these molecules and the resulting thermal distribution of conformers in solution. Similarly, the width of the fluorescence band increases strongly from **P** to **BPh-P**. It is interesting to note that the fluorescence spectra of **P** and **Ph-P** measured in the nonpolar cyclopentane (data not presented) show differences in the vibrational structure (compared to the spectra shown in Figure 3) but no overall solvatochromic shift could be observed. In contrast, the fluorescence of **BPh-P** is clearly Stokes shifted by ∼7 nm when changing the solvent from cyclopentane to acetonitrile. This indicates a difference in the dipole moments between the ground state and the emitting excited state of BPh-P.

**B. Femtosecond Time-Resolved Broad-Band Pump−Probe Spectra.** Figure 4 shows the temporal evolution of the pump−probe spectra of pyrene (**P**) after excitation at 334 nm. Note that around time-zero a sharp transient absorption band at 580 nm rises within the time resolution of our experimental setup. Delayed by several tens of femtoseconds, a second band is rising around 470 nm. It has been previously reported that excitation at 340 nm populates the $S_2$ state, which has an absorption band with a maximum at 580 nm.[43] This state undergoes ultrafast internal conversion into the $S_1$ state of pyrene, which exhibits a characteristic transient absorption band around 460 nm.[44,45] A rate constant of 150 ± 50 fs for this transition has been determined by Foggi et al.[43] In Figure 5 we display the time-dependent change of optical density at 580 and 450 nm. The filled circles represent the data that were obtained using a 100 $\mu$m thick cell. To directly compare the influence of the optical path length on the overall time resolution, we also show the corresponding measurement at 580 nm in a cell with a thickness of 1 mm. The data were analyzed by least-squares fitting as described in section II. For the 100 $\mu$m cell measurement we obtained an experimental response $\tau_M = 74$ fs and a decay constant of 78 fs. Using the 1 mm cell, one obtains a value of $\tau_M = 125$ fs and a decay constant of 89 fs. Even in the 100 $\mu$m cell the decay constant is very similar to the experimental response time. However, the asymmetric shape of the decay profile gives a clear indication that the decay constant is slightly longer or equal to the experimental response time. We, therefore, conclude that the $S_2 \rightarrow S_1$ IC process in **P** takes ∼75 fs.

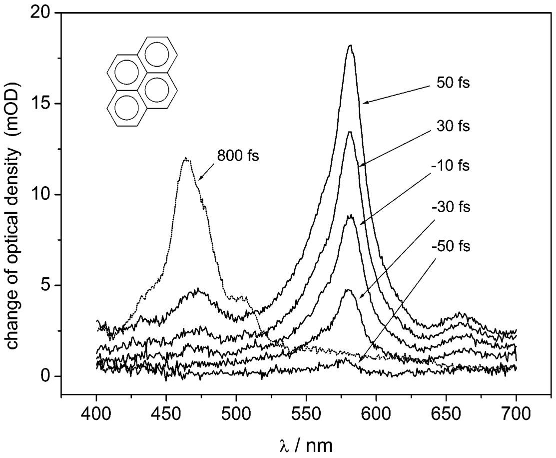

**Figure 4.** Femtosecond time-resolved pump−probe spectra of pyrene (**P**) in acetonitrile in the time range of −50 to 800 fs.

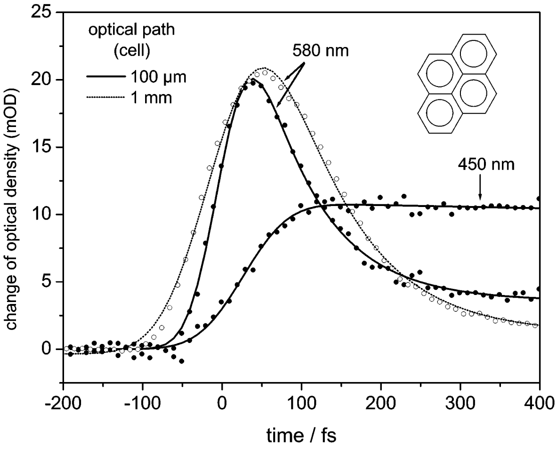

**Figure 5.** Femtosecond time-resolved transient absorption of the $S_2 \rightarrow S_n$ (580 nm) and $S_1 \rightarrow S_n$ (450 nm) states of pyrene in acetonitrile after excitation at 337 nm.

Figure 6 displays the time-dependent pump−probe spectra of **Ph-P** in acetonitrile after excitation at 345 nm. In contrast to the spectra of **P** (see Figure 4**),** the transient spectra of **Ph-P** show two absorption bands at early time; that is, in addition to the well-known $S_2 \rightarrow S_n$ absorption, there is a second maximum located at ∼640 nm. Since both absorption bands exhibit the same time-dependent behavior, they must be interpreted as two absorption transitions from the $S_2$ state. The characteristic pyrene $S_1$ absorption band is rising—with a certain time delay—between

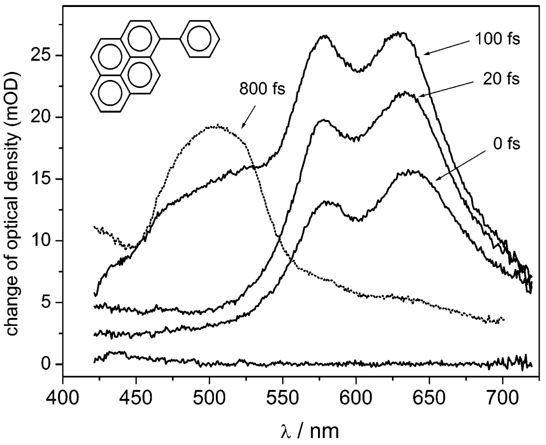

**Figure 6.** Femtosecond time-resolved pump−probe spectra of **Ph-P** in acetonitrile in the time range of 0 to 800 fs. The excitation wavelength was 345 nm.

470 and 550 nm. The maximum of the S$_1$ absorption band is shifted by more than 30 nm. As observed in the ground-state absorption spectra, it is noticeable that both the S$_1$ and the S$_2$ absorption bands are significantly broadened compared to the ones of pyrene. In addition, there are differences in the line shape, in particular for the S$_2$ state absorption bands of **P** and **Ph-P**. Whereas the S$_2$ absorption profile of **P** has a Lorentzian shape, the two S$_2$ absorption peaks in **Ph-P** can be well described as Gaussians. The Gaussian line shape indicates inhomogeneous broadening and is expected for a sample with a thermally averaged distribution of subensembles having different twisting angles. The possibility to characterize the line shape of transient absorption bands is a clear advantage of the broad-band detection mode and provides important details about the microscopic homogeneity of the systems studied.

Despite the spectral differences of **P** and **Ph-P**, one observes the same dynamical behavior for the two systems: The initial population of the S$_2$ state is followed by ultrafast internal conversion which can be monitored by both the decay of the S$_2$ band and the rise of the S$_1$ pyrene type absorption band. Although we were able to obtain a shorter temporal response function at 345 nm ($\tau_M = 50$ fs), it was not possible to accurately resolve the S$_1$ decay rate in **Ph-P** (see Figure 8). From the fit we received a value for the decay constant at 650 nm $<$ 50 fs. This is shorter than the experimental response and can therefore only be taken as an upper limit for the actual decay constant.

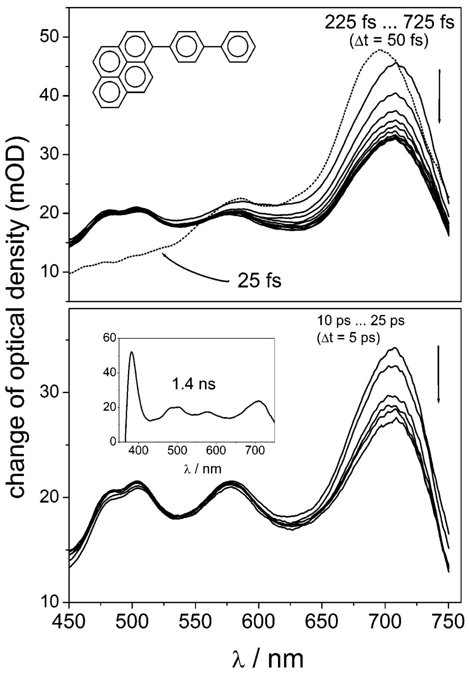

**Figure 7.** Femtosecond time-resolved pump−probe spectra of **BPh-P** in acetonitrile in the short time range (upper panel, 225 to 775 fs in 50 fs steps) and in the long time range (lower panel, 10 to 50 ps in 5 ps steps). The excitation wavelength was 345 nm. The inset displays the pump−probe spectrum 1.4 ns after excitation in a larger spectral range. The peak at 380 nm belongs to the S$_1 \rightarrow$ S$_n$ spectrum of pyrene (see text).

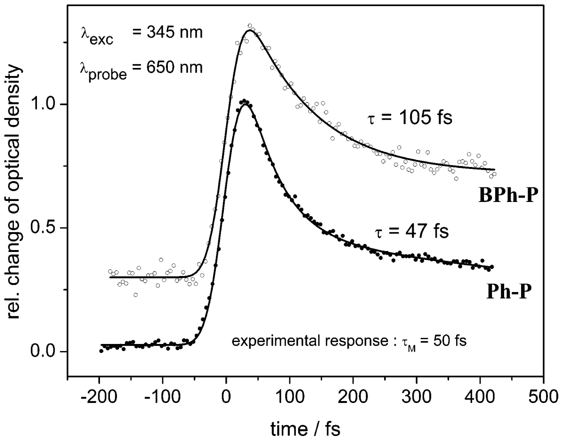

**Figure 8.** Time-resolved transient absorption of **Ph-P** and **BPh-P** in acetonitrile, probed at 650 nm. An experimental response time (Gaussian) of $\tau_M = 50$ fs was determined from the fit of the data (see text).

Figure 7 shows the time-dependent absorption spectra of **BPh-P** in acetonitrile. At early times (upper panel) one observes two initial absorption bands, similar to those in **Ph-P** but with very different absorption coefficients. The pyrene type S$_2$ absorption band (580 nm) can be recognized, although it is less pronounced and masked by a broad spectral background. The main absorption band at early times has a maximum around 700 nm. As observed for **Ph-P**, the characteristic absorption band of the S$_1$ state rises with a certain delay. However, one can observe a drastic difference in the time evolution of the spectral components. Both initial absorption peaks (at 580 and 705 nm), which must be assigned to transitions from the S$_2$ state, show an incomplete decay. Thus, there is a remaining contribution from the spectrum of the initially excited state to the spectrum of the relaxed S$_1$ state. Monitoring the time-dependent spectra at longer times reveals that this contribution remains present in the spectrum for at least several nanoseconds (the lifetime of the S$_1$ state is estimated to be $>$10 ns). The inset of Figure 7 shows the relaxed S$_1 \rightarrow$ S$_n$ spectrum 1.4 ns after excitation. Note that there is a strong absorption peak at 380 nm which is characteristic for the S$_1 \rightarrow$ S$_n$ absorption spectrum of pyrene.[44] The presence of this peak rules out that intramolecular charge transfer—which would lead to pyrene radical ions—is a dominant relaxation channel in **BPh-P**. Figure 8 shows the temporal evolution of the transient absorption at 650 nm for **Ph-P** and **BPh-P**. Clearly, the decay dynamics are slower in **BPh-P** (105 fs) than in **Ph-P** ($\leq$ 50 fs). It is important to emphasize that we obtained the same decay constant of 105 fs also at 580 nm, whereas the 705 nm band of **BPh-P** decays significantly more slowly (145 fs, data not shown).

**C. Sample Selection, Experimental Conditions, and Time Resolution.** Femtosecond spectroscopy in the condensed phase requires optical cells with short path length to minimize time broadening of the response function due to (i) group velocity mismatch, (ii) dispersion in the solvent, and (iii) the pump−

probe beam interaction geometry.[46,47] As a result, many femtosecond experiments are carried out in thin films or in solvent jets. The chemical systems that have been studied are often selected with respect to their absorption coefficients to achieve large excited state populations and sufficiently high signal-to-noise ratios for the observed transients. However, many molecular systems of interest, especially with biological relevance, have moderate to low extinction coefficients. As a result, one has to increase the concentration in the sample to achieve reasonably high absorbance over a very thin optical path. This approach often leads to drastic changes in the microscopic environment due to intermolecular interaction like stacking and aggregation. Although excimer formation is a diffusion-controlled process, which occurs typically on the time scale of 100 ps, it cannot be excluded that significant ground-state interactions are already present at these high concentrations. Evidence for the onset of aggregation between pyrene molecules may be found by comparing the data in Figure 5 where 400 fs after excitation the remaining long-lived spectral component (at 580 nm) in the 100 $\mu$m cell measurement is more than twice the value which is observed in the 1 mm cell data. Transient absorption spectra of pyrene excimers show an increased absorption in this spectral range.[48]

Our experiments suggest that, depending on the scientific question of interest, it may be reasonable to trade in time resolution for maintaining realistic (and relevant) sample conditions with respect to intermolecular interactions and environmental effects.

## IV. Discussion

**A. Femtosecond Excited-State Dynamics in Substituted Pyrenes.** By comparing both the steady state and the time-resolved spectroscopic data for the three pyrene derivatives, significant differences in their photophysical properties become apparent. These differences must be viewed in the context of effects on the electronic structure of pyrene induced by the aryl substituents. There are two effects that need to be considered. First, the molecular symmetry of pyrene (point group: $D_{2h}$) is reduced to $C_1$ by the introduction of an aryl substituent in the 1-position, which influences the vibrational modes and therefore the vibronic coupling between the $S_2$ and the $S_1$ states. Second, the $\pi$-electron substituent interacts with the $\pi$-electronic system of pyrene, which causes alterations of the excited-state energies. Both effects will have a direct influence on the $S_2 \rightarrow S_1$ internal conversion rate.

Fluorescence excitation spectra of pyrene in the gas phase[29,30] have shown a so-called intermediate-level structure;[49] that is, the $S_2$ vibronic levels are diluted among a manifold of distinct molecular eigenstates. Such complex fine-structured spectra are characteristic for molecules with small $S_2-S_1$ electronic energy gaps. In accord with the energy gap law which predicts the rates of radiationless transitions in polyatomic molecules,[31] one would expect an ultrafast IC process and therefore an ultrashort lifetime of the $S_2$ state. From measurements of the $S_2$ fluorescence of pyrene in the vapor phase,[50] the $S_2$ state lifetime was estimated by Ohta et al. to be between 50 and 100 fs.[30] Furthermore, from the width of the fluorescence excitation line shape it was concluded that intramolecular vibrational energy redistribution (IVR) in the $S_1$ state occurs with a time constant of 1 ps. Hence, population recurrences during the $S_1$ state lifetime should be expected in the gas phase.[30]

The femtosecond time-resolved data presented in this paper are entirely consistent with earlier high-resolution spectroscopy studies. The actual $S_2 \rightarrow S_1$ IC rate of ~75 fs for pyrene agrees well with the estimation from Ohta et al. The fact that our data have not shown evidence for population recurrence from the $S_1$ to the $S_2$ state underlines the special influence of the solvent on the excited-state relaxation. In addition to IVR, which may also be altered by the interaction with the solvent, the energy is rapidly dissipated by solvent modes (vibrational relaxation, VR), leading to an irreversible IC process. Furthermore, the role of the solvent is prominent in the homogeneous line broadening of the vibronic $S_0 \rightarrow S_2$ transitions in the ground-state absorption spectrum. An upper limit of ~12 fs for the time scale of phase relaxation induced by solvent fluctuations can be estimated from the Lorentzian shape line width (450 $cm^{-1}$).

Introducing a phenyl substituent to pyrene reduces the molecular symmetry and relaxes, therefore, the strict selection rules for vibronic coupling. The low-frequency interchromophore twisting mode in **Ph-P** can efficiently couple to solvent modes. Due to this broadening the $S_2-S_1$ Franck−Condon overlap should be very large for this mode. Consequently, the short $S_2$ state lifetime can be explained solely on the basis of vibronic arguments. On the basis of the statistical and symmetry arguments, one could expect an even faster IC rate in **BPh-P** than in **Ph-P**. Instead, we observe a rate of ~105 fs, which is at least a factor of 2 slower than the one in **Ph-P**. This observation indicates that the IC dynamics depend also critically on the curvature and on the relative positions of the two potential energy surfaces, and thus on the electronic interaction between the $\pi$-subsystems. The latter point appears to be crucial for the dynamics of **BPh-P**. Here, the steady-state spectra give a clear evidence that the electronic structure of pyrene is significantly disturbed by the biphenyl substituent. Although the solvatochromic shift of **BPh-P** indicates a change in the electric dipole moments between $S_1$ and $S_0$ states, excited-state charge transfer can be ruled out as the dominant relaxation channel in **BPh-P** because of several reasons: (i) The steady-state spectra show only a mild solvent dependence that cannot account for an excited state with a large dipole moment; (ii) the typical pyrenyl $S_1 \rightarrow S_n$ band appears at 370 nm, and (iii) finally, unfavorable redox potentials.[51] Consequently, we do not expect to see contributions from pure CT states to the transient absorption spectra. However, the significant red shift in the absorption spectra of **Ph-P** and **BPh-P** (with respect to **P**) implicates electronic coupling between individual $\pi$-subunits. Directly linked chromophores are characterized by a unique mode of electronic interaction which is highly dependent on the torsional angle(s). The dependence results from the interchromophore orbital overlap integral, which is zero for $\pi$-electrons in a fully twisted 90° configuration.

In the following discussion we propose an adiabatic model based on superposition of "zero-order" states. This approach seems justified because of the dominant pyrene type spectral features which appear in both the steady-state and the time-resolved data of **Ph-P** and **BPh-P**. As previously derived for similar types of bichromophoric systems,[52,53] we express the two lowest excited states $\Psi_m$ ($m = 1$ and 2) in **Ph-P** and **BPh-P** as linear combinations of zero-order states:

$$\Psi_m = c_1^{(m)}|S_1^\circ\rangle + c_2^{(m)}|S_2^\circ\rangle + c_3^{(m)}|\mathrm{Exc}\rangle \qquad (4)$$

$S_1^\circ$ and $S_2^\circ$ represent the $S_1$ and $S_2$ states of the "unperturbed" pyrene. $|\mathrm{Exc}\rangle$ is an excitonic configuration which results mainly from $\pi$-orbital overlap between the aromatic subunits. For a bichromophoric system $C_1-C_2$, $|\mathrm{Exc}\rangle$ can be a mixture of low-lying LE and CT states: $|C_1{}^*-C_2\rangle$, $|C_1-C_2{}^*\rangle$, $|C_1{}^+-C_2{}^-\rangle$, and $|C_1{}^--C_2{}^+\rangle$. This model is supported by molecular orbital calculations which show that the $\pi$-orbitals are delocalized in

**Ph-P** and **BPh-P**. The degree of delocalization depends strongly on the twisting (dihedral) angle between pyrene and the aryl substituent. Extensive theoretical work by Scholes and Ghiggino has shown that delocalization is caused by interchromophore orbital overlap and "through-configuration" interactions.[6,7] The latter includes exciton transfer due to coherent (or virtual) two-electron exchange.

Note that eq 4 takes into account not only excitonic interactions but also the mixing between the two lowest excited pyrene states. This mixing is expected from alteration of the $S_2-S_1$ energy gap due to the substitution and the reduction of symmetry. The mixing coefficients $c$ are strongly dependent on the molecular structure and are, therefore, time-dependent, as discussed below.

The $S_2$ state spectrum of **Ph-P** can be assembled from $S_2^\circ$ and an additional band which originates from the bichromophoric coupling between the phenyl substituent and pyrene. Applying eq 4 therefore results in

For **Ph-P**:
$$|S_1\rangle \approx |S_1^\circ\rangle \qquad (5)$$

$$|S_2\rangle = c_1^{(2)}|S_2^\circ\rangle + c_2^{(2)}|\mathrm{Exc}\rangle \qquad (6)$$

The latter electronic configuration $|\mathrm{Exc}>$ is responsible for the absorption band around 640 nm. In fact, semiempirical ZINDO calculations confirm this interpretation.[54] By calculating the electronic transition dipole moments from both the $S_1$ and the $S_2$ state to the higher excited states, we were able to find distinct transitions which could be assigned to single electron excitations between moderately delocalized orbitals. The obtained wavelengths were in reasonable agreement with the observed transient spectra of **P**, **Ph-P**, and **BPh-P**. As the IC proceeds in **Ph-P**, both absorption bands decay and the typical $S_1$ state absorption appears (see Figure 6). From the temporal evolution of the transient absorption spectra, we can deduce the actual composition of the state wave function, since the oscillator strengths $f_{m,n}$ corresponding to eqs 5 and 6 are given by

$$f_{1,n} \propto |\langle S_1^\circ|\hat{\mu}|S_n\rangle|^2 \qquad (7)$$

$$f_{2,n} \propto |c_1^{(2)}\langle S_1^\circ|\hat{\mu}|S_n\rangle + c_2^{(2)}\langle \mathrm{Exc}|\hat{\mu}|S_n\rangle|^2 \qquad (8)$$

Here $\hat{\mu}$ is the electric dipole moment operator. Note that $S_n$ is generic for a higher excited singlet state rather than for a specific state.

A more complex mixing scheme can be found for **BPh-P**. Here, the $S_2$ state consists mainly of an excitonic absorption at 705 nm and a minor contribution from the pyrene type $S_2$ state.

For **BPh-P**:
$$|S_1\rangle = c_1^{(1)}|S_1^\circ\rangle + c_2^{(1)}|S_2^\circ\rangle + c_3^{(1)}|\mathrm{Exc}\rangle \qquad (9)$$

$$|S_2\rangle = c_1^{(2)}|S_2^\circ\rangle + c_2^{(2)}|S_1^\circ\rangle + c_3^{(2)}|\mathrm{Exc}\rangle \qquad (10)$$

$$f_{1,n} \propto |c_1^{(1)}\langle S_1^\circ|\hat{\mu}|S_n\rangle + c_2^{(1)}\langle S_2^\circ|\hat{\mu}|S_n\rangle + c_3^{(1)}\langle \mathrm{Exc}|\hat{\mu}|S_n\rangle|^2 \qquad (11)$$

$$f_{2,n} \propto |c_1^{(2)}\langle S_2^\circ|\hat{\mu}|S_n\rangle + c_2^{(2)}\langle S_1^\circ|\hat{\mu}|S_n\rangle + c_3^{(2)}\langle \mathrm{Exc}|\hat{\mu}|S_n\rangle|^2 \qquad (12)$$

Due to strong $S_2-S_1$ mixing, one can observe contributions from $|S_2^\circ\rangle$ and $|\mathrm{Exc}\rangle$ even in the relaxed $S_1$ state. However, in contrast to the case for **Ph-P**, the coefficients for **BPh-P** are time-dependent. The relative spectral contributions of $S_2^\circ$, $S_1^\circ$, and Exc are changing on the very short time scale during the actual IC process. In addition, the exciton interaction ($c_3$) is changing on a slower time scale of several picoseconds. The fact that the time constant for the ultrafast decay of the 705 nm band (145 fs) differs from the one for the band at 580 nm (105 fs) could be an indication for a mode-specific IC rate. However, one must be cautious with this interpretation, since it cannot be ruled out that the composition of the adiabatic $S_2$ state is changing as the system evolves along the relaxation pathway.

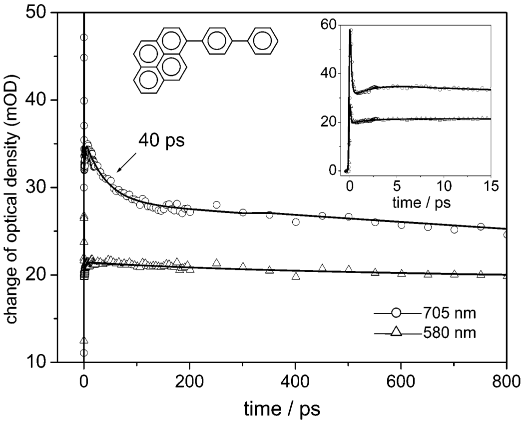

**Figure 9.** Time-resolved transient absorption of **BPh-P** in acetonitrile, probed at 705 and 580 nm. Inset: short time range. Excitation wavelength was 345 nm.

Figure 9 shows the time-resolved transient aborption at 580 and 705 nm. The inset displays a medium time range of up to 15 ps. The 705 nm band decays with a time constant of 40 ps, followed by a slower nanosecond decay. This picosecond time constant has not been observed for any other absorption band. It is plausible to assign these dynamics to structural relaxation in the $S_1$ state, which involves changes in the twisting angle(s) and therefore in the interchromophore coupling element $V$.

Directly linked multichromophoric molecules are expected to undergo structural changes in the excited state.[55] Generally, they tend to become more planar than those in the ground state due to resonance interactions, as exemplified for biphenyl and its methyl derivatives.[56] However, for some molecular systems the opposite trend—which leads to a twisted intramolecular charge transfer state (TICT)—has been proposed.[57] Femtosecond broad-band pump−probe spectra should be very sensitive toward twisting and planarization, since these motions control directly the degree of $\pi$-electron delocalization, which in turn determines the transient absorption properties.[19] Therefore, the 40 ps decay of the 705 nm band in **BPh-P** may be interpreted as an intramolecular electronic decoupling due to twisting around the pyrene−biphenyl dihedral angle $\varphi$ (TICT formation). This assignment is in reasonable agreement with reported time constants for twisting in D/A substituted biphenyls and 9,9′-bianthryl which are on the order of 10 ps.[58,59]

According to the above model, the absorption coefficient for the 705 nm band, $\epsilon_{705}$, should depend on the mixing and therefore on the coupling matrix element $V$. As proposed earlier by Dogonadze et al.,[60] the coupling element is proportional to the $\pi$-electron overlap between pyrene and the biphenyl moiety. As a result, $V$ is directly related to the $\varphi$: $V \propto \cos(\varphi)$. Since $\epsilon_{705}$ is proportional to $V^2$, we can estimate the value for the new angle $\varphi'$ after structural relaxation if $\varphi$ is known.

$$\frac{\cos^2(\varphi)}{\cos^2(\varphi')} = \frac{\epsilon_{705}(\varphi)}{\epsilon_{705}(\varphi')} \qquad (13)$$

From AM1 calculations of the ground state of **BPh-P** we obtained a value of 57° for $\varphi$. From the inset of Figure 9 one can see that after the IC process is completed, there is a slight rise of $\epsilon_{705}$ on the time scale of 2 ps. Using eq 14, this corresponds to a reduction of $\varphi$ by $\sim 2°$. After the initial planarization in the $S_1$ state, **BPh-P** undergoes twisting; this process takes place with a time constant of 40 ps. If $\varphi$ is 55°, a change of only 4.8° ($\varphi' = 59.8°$) can cause the observed decrease in the absorption band at 705 nm. Note that this interpretation is entirely consistent with the observed solvatochromic shift in the fluorescence of **BPh-P**, which indicates emission from a partial charge transfer state which is likely to have a more twisted structure than **BPh-P** in its unrelaxed $S_1$.

The femtosecond time-resolved spectral evolution clearly demonstrates that the individual electronic contributions evolve separately with time. This observation implies that the perturbation of the main chromophore (pyrene) by aryl substituents is so significant that the pure chromophore states cannot serve as reference states to characterize the ultrafast electronic relaxation process. The relevance of this observation for modeling electron-transfer processes in multichromophore assemblies will be discussed below.

**B. Intramolecular Exciplexes and Charge Transfer States.** Directly linked conjugated aromatic systems built from non-identical $\pi$-systems have similar properties to those of $\pi$-stacked intermolecular exciplexes.[61,62] In both classes of systems the electronic coupling results in partial charge transfer and exciton interactions between locally excited states. Spectroscopically, one can observe this mixed character both in fluorescence (exciplex emission) and in excited-state absorption measurements. The latter are less often reported because they are more difficult to monitor. Characterizing exciplex absorption bands by similar means as applied to fluorescence bands requires a very high experimental sensitivity as well as a broad-band probing technique. Since exciplex absorption may represent a reverse optical charge transfer (OCT) in the excited state,[19] it is interesting to compare the line shape parameters with those obtained from the recombination fluorescence. Studies on several strongly coupled organic charge transfer systems which exhibit reverse OCT absorption bands are currently being carried out in our laboratory.

Finally, we want to address the implication of time-dependent excited state mixing for ultrafast electron transfer processes. Our results have shown that the electronic structure of pyrene is significantly perturbed by aromatic substituents. Perturbation effects of conjugated substituents on the electronic structure in chromophores are well-known since the early days of molecular orbital theory.[63,64] In multidimensional D/A arrays where the initially excited state is spread out over more than one $\pi$-system, the effect on the energetics of the electron-transfer process can be accounted for by using empirical corrections for ionization potentials and electron affinities. Recently, conventional electron transfer theory[65−67] has been extended for such delocalization effects.[68,69] If, however, the delocalization over adjacent $\pi$-systems (within the LE state) is a *dynamical* process which occurs on the same time scale as the electron transfer, the simple diabatic two-state model does not apply. In this case, the electronic structure of the LE state as well as the resulting rates for electron transfer become time-dependent. Such a situation—which may be present in many femtosecond charge transfer processes in conjugated D/A arrays—requires a more advanced theoretical description which goes beyond the classical diabatic two-state model.

**Acknowledgment.** The work was supported by the Deutsche Forschungsgemeinschaft (Emmy-Noether Program Fi-721/3-1, 3-4), by the Volkswagen Stiftung, and by the Fonds der Chemischen Industrie. We warmly thank Dr. W. Kühnle (MPI Göttingen) for the synthesis, characterization, and purification of 1-phenylpyrene. We are also grateful to Dr. Roman Ioussoupov and Pancho Tzankov for experimental assistance. We would also like to thank the two reviewers for their thoughtful suggestions to improve the manuscript.

**Supporting Information Available:** The synthesis of 1-biphenyl-4-yl-pyrene (**BPh-P**). This material is available free of charge via the Internet at http://pubs.acs.org.

## References and Notes

(1) *Electron Transfer in Chemistry, Vol. 5*; Balzani, V., Ed.; Wiley-VCH: Weinheim, 2001.

(2) *Molecular Electronics: Science and Technology*; Aviram, A., Ratner, M., Eds.; New York Acadamy of Sciences: New York, 1998; Vol. 852.

(3) Strachan, J.-P.; Gentemann, S.; Seth, J.; Kalsbeck, W. A.; Lindsey, J. S.; Holton, D.; Bocian, D. F. *J. Am. Chem. Soc.* **1997**, *119*, 11191.

(4) Scholes, G. D.; Ghiggino, K. P. *J. Photochem. Photobiol. A* **1994**, *80*, 355.

(5) Scholes, G. D. *J. Phys. Chem.* **1996**, *100*, 18731.

(6) Scholes, G. D.; Ghiggino, K. P. *J. Chem. Phys.* **1994**, *101*, 1251.

(7) Harcourt, R. D.; Scholes, G. D.; Ghiggino, K. P. *J. Chem. Phys.* **1994**, *101*, 10521.

(8) *Femtosecond Chemistry*; Manz, J., Wöste, L., Eds.; VCH: Weinheim, 1995; Vols. 1 and 2.

(9) Zewail, A. H. *J. Phys. Chem. A* **2000**, *104*, 5660.

(10) Förster, T.; Kasper, K. *Z. Phys. Chem. N. F.* **1954**, *1*, 275.

(11) Werner, H.-J.; Staerk, H.; Weller, A. *J. Chem. Phys.* **1978**, *68*, 2419.

(12) Staerk, H.; Kühnle, W.; Treichel, R.; Weller, A. *Chem. Phys. Lett.* **1985**, *118*, 19.

(13) Wynne, K.; Reid, G. D.; Hochstrasser, R. M. *J. Chem. Phys.* **1996**, *105*, 2287.

(14) Fiebig, T.; Kühnle, W.; Staerk, H. *J. Fluoresc.* **1997**, *7*, 29S.

(15) Fidler, V.; Kapusta, P.; Nepras, M.; Schroeder, J.; Rubtsov, I. V.; Yoshihara, K. *Collect. Czech. Chem. Commun.* **1998**, *63*, 1460.

(16) Mataga, N.; Miyasaka, H. Electron Transfer and Exciplex Chemistry. In *Electron Transfer: From Isolated Molecules to Biomolecules, Part Two*; Jortner, J., Bixon, M., Eds.; John Wiley & Sons: New York, 1999; p 431.

(17) Daub, J.; Engl, R.; Kurzawa, J.; Miller, S. E.; Schneider, S.; Stockmann, A.; Wasielewski, M. R. *J. Phys. Chem. A* **2001**, *105*, 5655.

(18) Fiebig, T.; Stock, K.; Lochbrunner, S.; Riedle, E. *Chem. Phys. Lett.* **2001**, *345*, 81.

(19) Pandurski, E.; Fiebig, T. *Chem. Phys. Lett.* **2002**, *357*, 272.

(20) Dobkowski, J.; Rettig, W.; Waluk, J. *Phys. Chem. Chem. Phys.* **2002**, *4*, 4334.

(21) Shafirovich, V. Y.; Courtney, S. H.; Ya, N.; Geacintov, N. E. *J. Am. Chem. Soc.* **1995**, *117*, 4920.

(22) Netzel, T. L.; Nafisi, K.; Headrick, J.; Eaton, B. E. *J. Phys. Chem.* **1995**, *99*, 17948.

(23) Lewis, F. D.; Zhang, Y.; Letsinger, R. L. *J. Am. Chem. Soc.* **1997**, *119*, 5451.

(24) Masuko, M.; Ohtani, H.; Ebata, K.; Shimadzu, A. *Nucleic Acids Res.* **1998**, *26*, 5409.

(25) Amann, N.; Pandurski, E.; Fiebig, T.; Wagenknecht, H.-A. *Angew. Chem., Int. Ed.* **2002**, *41*, 2978.

(26) Amann, N.; Pandurski, E.; Fiebig, T.; Wagenknecht, H.-A. *Chem. Eur. J.*, in press.

(27) Birks, J. B. *Photophysics of Aromatic Molecules*; Wiley-Interscience: New York, 1970.

(28) Marconi, G.; Salvi, P. R. *Chem. Phys. Lett.* **1986**, *123*, 254.

(29) Mangle, E. A.; Topp, M. R. *J. Phys. Chem.* **1986**, *90*, 802.

(30) Ohta, N.; Baba, H.; Marconi, G. *Chem. Phys. Lett.* **1987**, *133*, 222.

(31) Englman, R.; Jortner, J. *Mol. Phys.* **1970**, *18*, 145.

(32) Dobkowski, J.; Waluk, J. *Pol. J. Chem.* **1993**, *67*, 1389.

(33) Martinez, O. E.; Gordon, J. P.; Fork, R. L. *Opt. Lett.* **1984**, *1*, 1003.

(34) Wurzer, A. J.; Lochbrunner, S.; Riedle, E. *Appl. Phys. B* **2000**, *71*, 405.

(35) Albrecht, T. F.; Siebert, K.; Kunz, H. *Opt. Commun.* **1991**, *84*, 223.

(36) Tokunaga, E.; Terasaki, A.; Kobayashi, T. *Opt. Lett.* **1993**, *18*, 370.

(37) Fork, R. L.; Shank, C. V.; Hirlimann, C.; Yen, R.; Tomlinson, W. J. *Opt. Lett.* **1983**, *8*, 1.

(38) Kovalenko, S. A.; Dobryakov, A. L.; Ruthmann, J.; Ernsting, N. P. *Phys. Rev. A* **1999**, *59*, 2369.

(39) Ekvall, K.; Meulen, P. v. d.; Dhollande, C.; Berg, L.-E.; Pommeret, S.; Naskrecki, R.; Mialocq, J.-C. *J. Appl. Phys.* **2000**, *87*, 2340.

(40) Lorenc, M.; Ziolek, M.; Naskrecki, R.; Karolczak, J.; Kubicki, J.; Maciejewski, A. *Appl. Phys. B* **2002**, *74*, 19.

(41) Above 650 nm in the WLC the XPM artifact signal was broadened and decreased in magnitude. To extend the range of the chirp measurement to 730 nm (while keeping the same relative accuracy of the XPM artifact measurement), we had to further compress the pump pulse.

(42) The time vector of the measured data is shifted for each wavelength according to the measured chirp. For the new time points we linearly interpolate the OD values between the OD values of the corresponding nearest neighbor time points.

(43) Neuwahl, F. V. R.; Foggi, P. *Laser Chem.* **1999**, *19*, 375.

(44) Richards, J. T.; West, G.; Thomas, J. K. *J. Phys. Chem.* **1970**, *74*, 4137.

(45) Foggi, P.; Pettini, L.; Sànta, I.; Righini, R.; Califano, S. *J. Phys. Chem.* **1995**, *99*, 7439.

(46) Ziolek, M.; Naskrecki, R.; Lorenc, M.; Karolczak, J.; Kubicki, J.; Maciejewski, A. *Opt. Commun.* **2001**, *197*, 467.

(47) Diels, J.-C.; Rudolph, W. *Ultrashort Laser Pulse Phenomena*; Academic Press: San Diego, CA, 1996.

(48) Post, M. F. M.; Langelaar, J.; Voorst, J. D. W. V. *Chem. Phys. Lett.* **1971**, *10*, 468.

(49) Mukamel, S.; Jortner, J. In *International Reviews of Science Physical Chemistry, Volume on Theoretical Chemistry*; Buckingham, A. D., Coulson, C. A., Eds.; Butterworth: London, 1975; p 391.

(50) Baba, H.; Nakajima, A.; Aoi, M.; Chihara, K. *J. Chem. Phys.* **1971**, *55*, 2433.

(51) Streitwieser, A. *Molecular Orbital Theory for Organic Chemists*; J. Wiley & Sons Inc.: New York and London, 1961.

(52) Tominaga, K.; Walker, G. C.; Jarzeba, W.; Barbara, P. F. *J. Phys. Chem.* **1991**, *95*, 10475.

(53) Scholes, G. D.; Fournier, T.; Parker, A. W.; Phillips, D. *J. Chem. Phys.* **1999**, *111*, 5999.

(54) Fiebig, T. Unpublished results.

(55) *Conformational Analysis of Molecules in Excited States*; Waluk, J., Ed.; Wiley-VCH: New York, 2000.

(56) Suzuki, H. *Electronic Absorption Spectra and Geometry of Organic Molecules*; Academic Press Inc.: New York, 1967.

(57) Grabowski, Z. R.; Rotkiewicz, K.; Siemiarczuk, A.; Cowley, D. J.; Baumann, W. *Nouv. J. Chim.* **1979**, *3*, 443.

(58) Maus, M.; Rettig, W.; Jonusauskas, G.; Lapouyade, R.; Rulliere, C. *J. Phys. Chem. A* **1998**, *102*, 7393.

(59) Mataga, N.; Nishikawa, S.; Okada, T. *Chem. Phys. Lett.* **1996**, *257*, 327.

(60) Dogonadze, R. R.; Kutznetsov, A. M.; Marsagishvili, T. A. *Electrochim. Acta* **1980**, *25*, 1.

(61) Verhoeven, J. W.; Scherer, T.; Willemse, R. J. *Pure Appl. Chem.* **1993**, *65*, 1717.

(62) Haar, T. v. d.; Hebecker, A.; Il'ichev, Y.; Jiang, Y.-B.; Kühnle, W.; Zachariasse, K. A. *Recl. Trav. Chim. Pays-Bas* **1995**, *114*, 430.

(63) Salem, L. *The Molecular Orbital Theory of Conjugated Systems*; W. A. Benjamin, Inc.: New York, 1966.

(64) Heilbronner, E.; Bock, H. *Das HMO−Modell und seine Anwendung*; Verlag Chemie: Weinheim, 1978.

(65) Marcus, R. A.; Sutin, N. *Biochim. Biophys. Acta* **1985**, *811*, 265.

(66) Brunschwig, B. S.; Sutin, N. Reflections on the Two-state Electron-transfer Model. In *Electron Transfer in Chemistry*; Balzani, V., Ed.; Wiley-VCH: Weinheim, New York, 2001; Vol. 2; p 583.

(67) Barbara, P. F.; Meyer, T. J.; Ratner, M. A. *J. Phys. Chem.* **1996**, *100*, 13168.

(68) Matyushov, D. V.; Voth, G. A. *J. Phys. Chem. A* **2000**, *104*, 6470.

(69) Matyushov, D. V.; Voth, G. A. *J. Phys. Chem. A* **2000**, *104*, 6485.